Geomechanics and Engineering, *Vol. 26, No. 4 (2021) 401-413*
https://doi.org/10.12989/gae.2021.26.4.401

Optimal design of mixing ratios of modifiers for disintegrated carbonaceous mudstone

Ling Zeng[1a], Huan-Yi Zha[1b] and Qian-Feng Gao*[2]

[1]*School of Civil Engineering, Changsha University of Science & Technology, 960, Section 2, Wanjiali South Road, Changsha 410114, Hunan, China*
[2]*School of Traffic & Transportation Engineering, Changsha University of Science & Technology, 960, Section 2, Wanjiali South Road, Changsha 410114, Hunan, China*

(Received October 24, 2019, Revised July 5, 2021, Accepted August 10, 2021)

Abstract. Under the effect of load and seasonal rainfall, the disintegrated carbonaceous mudstone (DCM) softens and further disintegrates, causing large settlements and even collapses of the DCM embankments. For this reason, some treatments should be taken to improve the engineering performance of the DCM. In this study, four materials including sodium alginate (SA), calcium chloride ($CaCl_2$), bentonite and nano-Al_2O_3 were jointly used as modifiers to treat the DCM. The influences of each modifier component on the unconfined compressive strength (UCS), cohesion, angle of internal friction, and coefficient of permeability of the DCM were examined by unconfined compression tests, direct shear tests and permeability tests. The results demonstrated that with the addition of modifiers, the UCS, cohesion and angle of internal friction of the DCM are enhanced, whereas the coefficient of permeability is reduced. The sensitivity analysis showed that the dosage of SA is the dominating factor affecting the engineering performance of the DCM. Thus, special attention should be paid to the dosage of SA when improving the DCM. On the other hand, bentonite is the least important factor for most of the examined engineering properties among the four modifier components. An UCS value that is greater than 1500 kPa was selected as the evaluation criterion, and the stress-strain relationship and failure mode of each sample under unconfined compression were examined. On this basis, eight groups of satisfactory mixing ratios were obtained for the modification of the DCM. It is suggested that when designing mixing ratios of modifiers for the DCM, the recommended SA/DCM ratio is 4%-6%, but the quantities of $CaCl_2$, bentonite and nano-Al_2O_3 can be adjusted according to the needs and costs.

Keywords: embankment; ground improvement; laboratory analysis; optimization; rock fills; shear strength

1. Introduction

In highway engineering, it is a general principle to preferentially use local materials as embankment fillers to reduce the project cost. In southern China, carbonaceous mudstone is widely distributed. This mudstone is a type of soft rock that is easy to disintegrate under the influence of rainwater, leading to a significant reduction in its mechanical strengths (Zeng *et al.* 2019, 2021a, b). The disintegration rate of this mudstone decreases as its grains become smaller (Zeng *et al.* 2017). Moreover, carbonaceous mudstone shows obvious dissolution, shrinkage and cracking characteristics because it contains a large number of hydrophilic clay minerals. Under repeated wet and dry actions, this material presents numerous longitudinal and transverse fissures (Zeng *et al.* 2019, Liu *et al.* 2017, Liu 2015). Thus, carbonaceous mudstone can never be used as an embankment filler unless it has already been disintegrated to some extent. The natural disintegration of carbonaceous mudstone is usually accompanied by the loss of clay minerals. As a result, this material exhibits similar characteristics as silty sand after disintegration. Nevertheless, although carbonaceous mudstone has been primarily disintegrated, it may undergo further disintegration under a long-term action of load and water immersion in the field. In this case, many engineering problems such as uneven settlement and insufficient bearing capacity of the embankments filled with this material are likely to occur (Zeng *et al.* 2019). Therefore, some treatments should be taken to improve the engineering performance of the disintegrated carbonaceous mudstone (DCM).

Some early studies reported that traditional cementitious materials show several limitations (e.g., easy-cracking, poor durability and environmental pollution) in the improvement of soft rock and soil (Voottipruex and Jamsawang 2014). From the 1990s, many scholars began to use new modifiers such as biological enzymes (Mujah *et al.* 2017, Xiao *et al.* 2017), geopolymers (Zhang *et al.* 2013), xanthan gum (Lee *et al.* 2017) and polymers (Rezaeimalek *et al.* 2017). However, these modifiers are also not widely used in engineering practice because of their high costs and complexity in construction. In recent years, with the increasing development of industry, the cost of industrial

*Corresponding author, Ph.D.
E-mail: qianfeng.gao@csust.edu.cn
[a]Ph.D.
E-mail: zl001@csust.edu.cn
[b]Ph.D. Student
E-mail: zhahy0326@stu.csust.edu.cn

ISSN: 2005-307X (Print), 2092-6219 (Online)

by-products has been greatly reduced, so environmentally friendly modifiers (e.g., plant cellulose, lignin and sodium alginate (SA)) have attracted much attention (Indraratna *et al.* 2012, Wen *et al.* 2019). For instance, the work of Zhang *et al.* (2018) revealed that under the same curing time and compaction conditions, 12% lignin is better than 8% cement in improving the mechanical performance of silty soil. Among the above three modifiers, plant cellulose and lignin are not suitable for improving the DCM because they have little contribution to the water stability of soil. As a natural polysaccharide polymer, SA shows a strong cementation effect and can improve the water-holding capacity of soil and the environment for plant growth (Geckil *et al.* 2010). Previous studies have reported that an addition of 3% biopolymers in soil exhibited equivalent modification effects as an addition of 10% cement (Chang *et al.* 2015). In other words, an appropriate amount of SA may be conducive to the engineering performance of the DCM. However, the availability of SA is limited due to its poor mechanical properties (Sarika and James 2016, Hecht and Srebnik 2016). To address this problem, some scholars suggested the addition of 1%-3% $CaCl_2$ to SA hydrogel since the products of the reaction between $CaCl_2$ and SA show better mechanical behavior than SA (Guo *et al.* 2016, Li *et al.* 2015). Moreover, Bhuvaneshwari *et al.* (2010) found that adding an appropriate amount of $CaCl_2$ could enhance the soil density, and thus, increase the soil strength. Bentonite is a clay mainly composed of montmorillonite, which is able to significantly reduce the permeability of soil (Benhouria *et al.* 2015, Taylor-Lange *et al.* 2015) and greatly adsorb metal cations in soil (Chai *et al.* 2017). Nano-Al_2O_3 has a large specific surface area and high activity, and it can also considerably enhance the mechanical behavior of soil (Luo *et al.* 2015, Gowda *et al.* 2017). Luo *et al.* (2012) investigated the effect of nano-Al_2O_3 on the unconfined compressive strength (UCS) of sludge mortar stabilized soil. It was found that a dosage of 1% nano-Al_2O_3 can lead to the largest UCS of the soil. Thus, SA, $CaCl_2$, bentonite and nano-Al_2O_3 may be selected as the components of modifiers for the DCM, but the gap of knowledge of the influence of each component on the engineering performance of the DCM and the optimal mixing ratios still need to fill.

In this study, the above four materials, i.e., SA, $CaCl_2$, bentonite, and nano-Al_2O_3, are jointly used to modify the engineering properties of the DCM. The influences of each material on the UCS, cohesion, angle of internal friction and coefficient of permeability of the DCM are examined, and the optimal mixing ratios are determined by the sensitivity analysis. The results can provide guidance for the treatment of the DCM in engineering practice.

2. Materials

2.1 Disintegrated carbonaceous mudstone

The studied carbonaceous mudstone is a weathered soft rock with fissure development. It was collected from a cut slope at the station K10+300 of the Liuzhou-Nanning highway in Liuzhou City, Guangxi Zhuang Autonomous Region, China. This region is in the subtropical monsoon climate with the most abundant rainfall in China. The annual precipitation of the region is more than 1070 mm, and most of the region has annual precipitation between 1,500 and 2,000 mm (Jin *et al.* 2017, Xiao *et al.* 2020). This region also shows obvious mountain climate features due to its mountainous and hilly landform. Since the DCM grains with sizes larger than 2 mm have the potential to undergo secondary disintegration, they are not recommended for embankment filling. Thus, the DCM grains not larger than 2 mm were used for testing in this study. The grain size distribution curve of the DCM is presented in Fig. 1. It shows that the DCM is mainly composed of sandy grains. The compaction tests revealed that the maximum dry density is 2.09 g/cm^3 and the optimum water content is 10.56%. The basic physical properties of the DCM are summarized in Table 1. X-ray diffraction (XRD) analysis indicated that the minerals of the DCM include kaolinite (38.27%), mica (29.54%), quartz (18.63%), pyrite (9.03%), etc. (Fig. 2). The chemical compositions are mainly Al_2O_3 and Fe_2O_3, among which Al_2O_3 accounts for 53.48%.

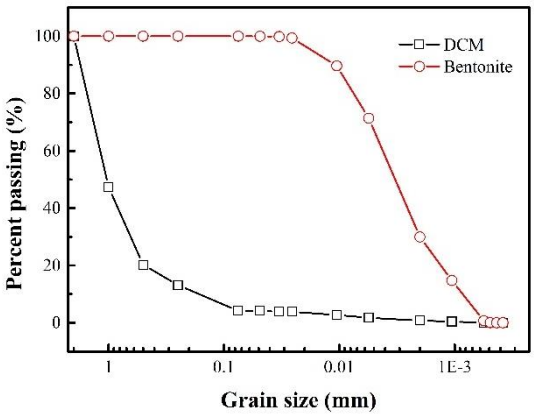

Fig. 1 Grain size distribution curves of the DCM and bentonite

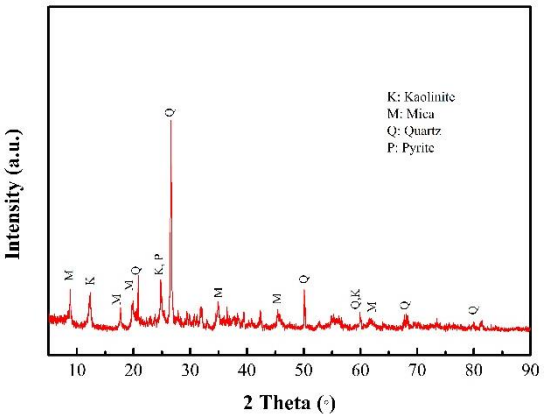

Fig. 2 XRD pattern of the DCM

2.2 Modifier components

SA, $CaCl_2$, bentonite and nano-Al_2O_3 were jointly used to prepare modifiers, as shown in Figs. 1(a)-1(d). SA was supplied by the Zhengzhou Chuangmei Chemical Products

(a) SA (b) $CaCl_2$ (c) Bentonite (d) Nano-Al_2O_3

Fig. 3 Photographs of the modifier components

Table 1 Physical properties of the DCM

Maximum dry density (g/cm^3)	Optimum water content (%)	Liquid limit (%)	Plastic limit (%)	Plasticity index	Specific gravity
2.09	10.6	32.9	25.3	7.6	2.66

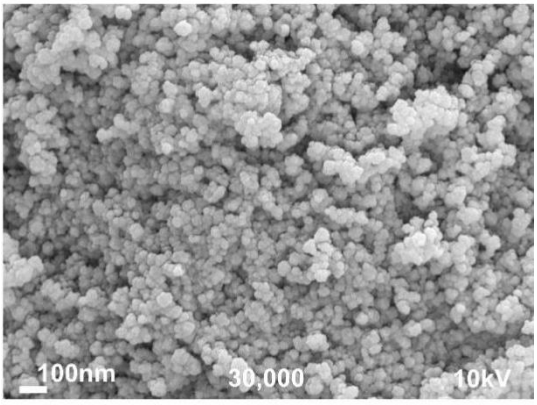

Fig. 4 SEM image of nano-Al_2O_3

Company (China). It is a yellow-brown powder with the chemical formula of $(C_6H_7NaO_6)_x$ (see Fig. 3(a)). The sieve analysis showed that most of the SA grains (93.1%) fall between 0.075 mm and 1 mm in size. $CaCl_2$ is an analysis reagent provided by the Sinopharm Chemical Reagent Co., Ltd. (China). It is a white granular material with a purity of up to 96% and a molecular weight of 110.98. Bentonite was produced by the Guangzhou Yifeng Chemical Technology Company (China). The bentonite particles are less than 0.075 mm, as shown in Fig. 1. Its liquid limit is 208.1%, plastic limit is 46%, and specific gravity is 2.70. Nano-Al_2O_3 is a white powder of high purity. The scanning electron microscopy (SEM) image of nano-Al_2O_3 in Fig. 4 shows that its grain sizes are 25 ± 5 nm.

3. Methodology

3.1 Orthogonal design

The orthogonal design is an efficient and economic method to arrange multi-factor and multi-level experiments. Because it often confounds interactions, it is especially used to identify the main influencing factors (Hu *et al.* 2018, Gao *et al.* 2019). In this study, the orthogonal design was performed to determine the optimal mixing ratios of modifier components for the DCM. Orthogonal array table L25 (5^6) was used. The SA/DCM ratio, $CaCl_2$/DCM ratio, bentonite/DCM ratio and nano-Al_2O_3/DCM ratio were selected as four influencing factors, and each factor had five levels: 0, 2%, 4%, 6% and 8% for the SA/DCM ratio; 0, 0.1%, 0.2%, 0.3% and 0.4% for the $CaCl_2$/DCM ratio; 0, 1%, 2%, 3% and 4% for the bentonite/DCM ratio; and 0, 1%, 2%, 3% and 4% for the nano-Al_2O_3/DCM ratio (Chang *et al.* 2015, Guo *et al.* 2016, Benhouria *et al.* 2015, Majeed *et al.* 2014, Tan *et al.* 2002) (see Table 2).

3.2 Sample preparation

The sample preparation can be divided into three steps, i.e., the mixing of materials, sample formation and sample curing.

- Mixing of materials

The DCM grains not larger than 2 mm were oven-dried at 106 °C for 24 h and then cooled down to the room temperature (20 ± 3 °C). According to the mixing ratios given in Table 2, many soil samples were prepared. In the first place, the DCM was mixed with SA and bentonite powder in a mixer for 10 min. Meanwhile, $CaCl_2$ was dissolved in a certain amount of deionized water (i.e., the water/DCM ratio = 10%). Then, nano-Al_2O_3 was dispersed in $CaCl_2$ solution using the ultrasonic dispersing device for 30 min. Afterward, the prepared solution was poured into the mixer containing the DCM, SA, and bentonite, and they were stirred for 30 min to obtain a homogeneous mixture. Because SA has the maximum solubility at about 60°C (Geckil *et al.* 2010), the temperature of the solution was maintained at 60°C during the stir. Finally, the prepared mixture was sealed with bags and cured for 24 h at the room temperature (Hataf *et al.* 2018, Kumar and Sujatha 2021).

- Sample formation

An appropriate amount of the mixture was filled into a cylindrical mold in three layers, and the material was compressed using the static compaction method. The samples had a diameter of 39.1 mm and a height of 80 mm for unconfined compression tests, a diameter of 61.8 mm and a height of 20 mm for direct shear tests, and a diameter of 61.8 mm and a height of 40 mm for permeability tests.

- Sample curing

Prior to testing, the prepared samples were cured. Existing studies showed that the strength of SA hydrogels is the largest when the curing temperature is 50°C (Indraratna

Table 2 Orthogonal design for the modification of the DCM

Case	Factor			
	SA/DCM ratio (%)	$CaCl_2$/DCM ratio (%)	Bentonite/DCM ratio (%)	Nano-Al_2O_3/DCM ratio (%)
T1	0	0	0	0
T2	0	0.1	1	1
T3	0	0.2	2	2
T4	0	0.3	3	3
T5	0	0.4	4	4
T6	2	0	1	2
T7	2	0.1	2	3
T8	2	0.2	3	4
T9	2	0.3	4	0
T10	2	0.4	0	1
T11	4	0	2	4
T12	4	0.1	3	0
T13	4	0.2	4	1
T14	4	0.3	0	2
T15	4	0.4	1	3
T16	6	0	3	1
T17	6	0.1	4	2
T18	6	0.2	0	3
T19	6	0.3	1	4
T20	6	0.4	2	0
T21	8	0	4	3
T22	8	0.1	0	4
T23	8	0.2	1	0
T24	8	0.3	2	1
T25	8	0.4	3	2

et al. 2012). In addition, the land surface temperature in southern China can reach 50-60 °C in summer. Thus, the samples for unconfined compression tests were cured first at a room temperature for 7 d and then at 50 °C for 48 h. The samples for direct shear tests and permeability tests were only cured at the room temperature for 7 d.

3.3 Test methods

Unconfined compression tests, direct shear tests and permeability tests were carried out on the cured samples to determine the UCS, cohesion, angle of internal friction and coefficient of permeability of the plain and modified DCM. Unconfined compression tests were performed at a constant loading rate of 1.5 %/min according to ASTM D2166 (2013). Direct shear tests were conducted in accordance with ASTM D6528-07 (2007). In direct shear tests, four normal stresses, i.e., 100 kPa, 200 kPa, 300 kPa and 400 kPa, were taken into consideration, and the shear rate was kept constant at 0.8 mm/min. The shear strength of a sample was defined as the peak shear stress on the displacement-shear stress plane. If there was no clear peak stress, the shear strength was defined as the shear stress corresponding to a horizontal displacement of 10 mm. Permeability tests were carried out using the falling-head method following the procedures recommended in ASTM D5084 (2016).

XRD and SEM tests were also conducted on the pieces extracted from the cylindrical samples to reveal the mechanism underlying the modification of DCM by the modifier. The XRD tests were performed in Phillips PW 3710 XRD system at 30 kV, 30 mA of CuKα radiation (l.5148 Å). The SEM observations was performed in a JSM-6490LV scanning electron microscope system (JEOL Corporation, Japan) at an accelerating voltage of 10 kV. A series of SEM images at different magnifications were saved for each DCM specimen (Gao *et al.* 2020, 2021).

4. Results and discussion

4.1 Test results

Fig. 5(a) shows the UCS, cohesion, angle of internal friction and coefficient of permeability of the DCM jointly modified by SA, $CaCl_2$, bentonite and nano-Al_2O_3 at various mixing ratios. It is noted that the UCS of the plain DCM (i.e., the sample without modification, case T1) is only 346.7 kPa. The UCSs of the DCM treated with the

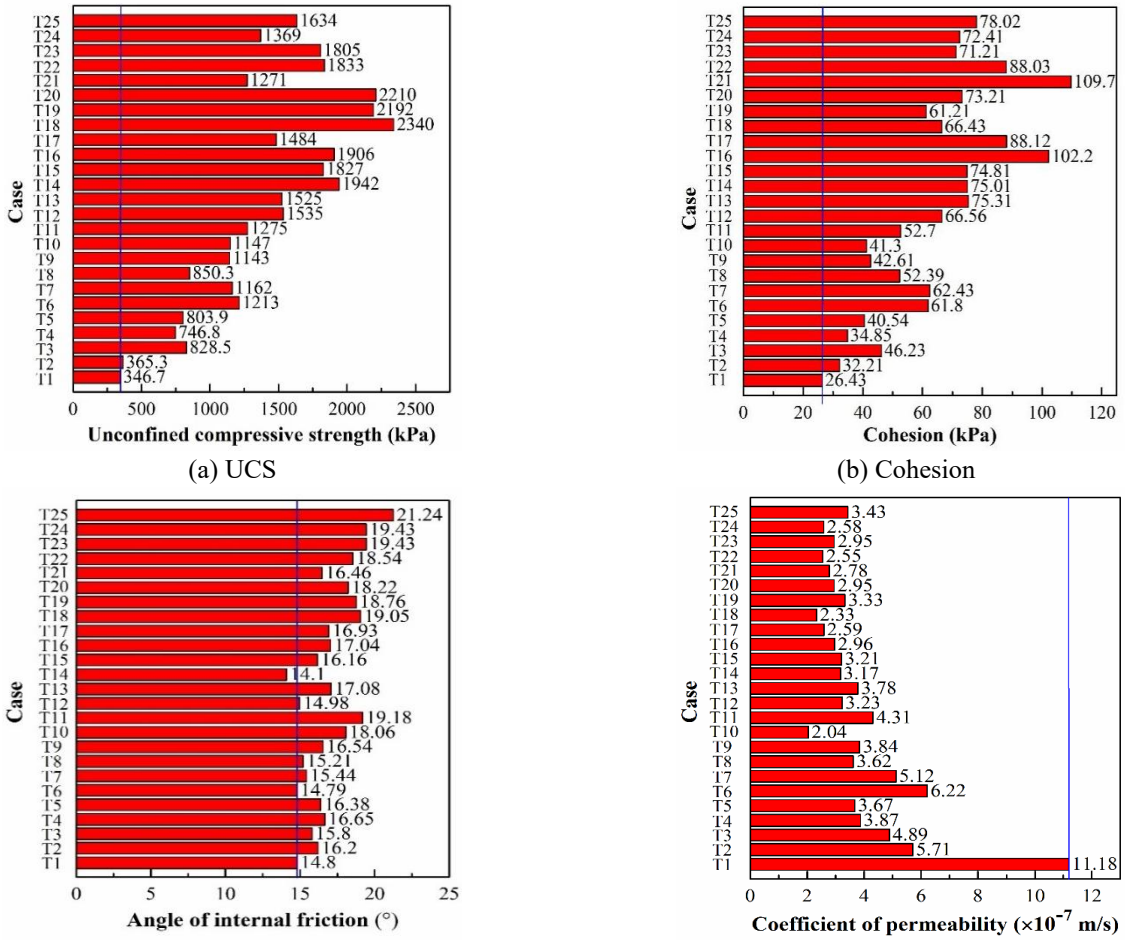

(a) UCS (b) Cohesion

(c) Angle of internal friction (d) Coefficient of permeability

Fig. 5 Effects of mixing ratios on the properties of the DCM

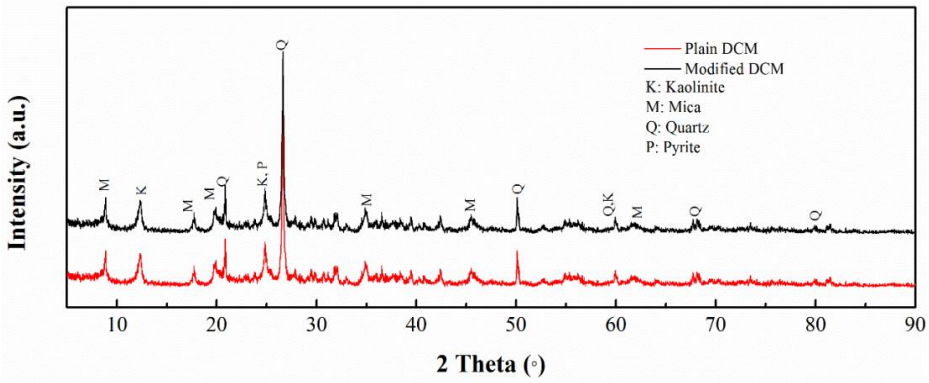

Fig. 6 XRD patterns of the plain and modified DCM

modifiers at various mixing ratios (cases T2-T25) are larger than 346.7 kPa, and the maximum UCS can reach as high as 2320.0 kPa in case T18. Compared with case T1, the UCS of the sample in case T18 increases by 569.17%. Fu *et al.* (2020) used cement and nano-Al_2O_3 to modify the DCM and found that the UCS of the modified DCM was only 1036 kPa when 8% cement or 0.2% nano-alumina was added alone, and the UCS reached the maximum of 1825 kPa when 8% cement and 0.2% nano-alumina were added together. Thus, compared with the modification based on cement and nano-Al_2O_3, the modification based on SA, $CaCl_2$, bentonite and nano-Al_2O_3 have greater advantages in enhancing the UCS of the DCM.

The cohesion of the plain DCM sample is 26.43 kPa, and the cohesion values of the DCM after adding modifiers are 32.21-109.7 kPa with increase rates of 21.87%-201.13% (Fig. 5(b)). It is noted that the sample in case T21 has the optimal mixing ratios for the improvement of the cohesion.

Fig. 5(c) shows the angles of internal friction. It can be seen that the angle of internal friction of the modified DCM

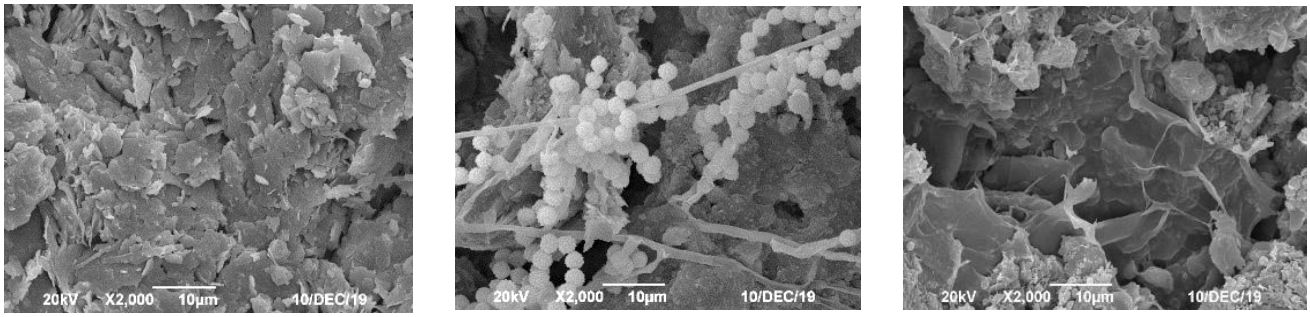

(a) Plain DCM (b) Modified DCM (c) Modified DCM

Fig. 7 SEM images of plain and modified DCM

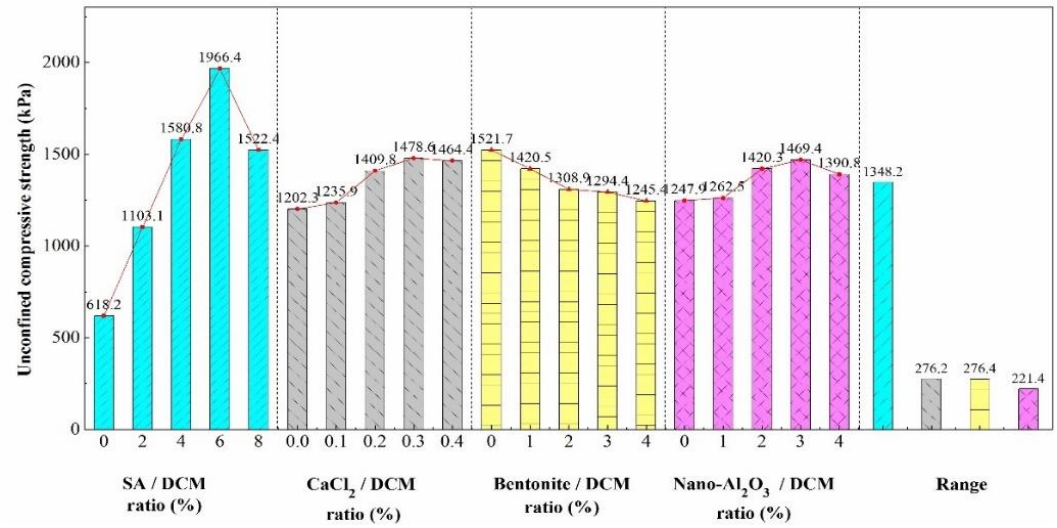

Fig. 8 Effects of mixing ratios on the UCS of the DCM

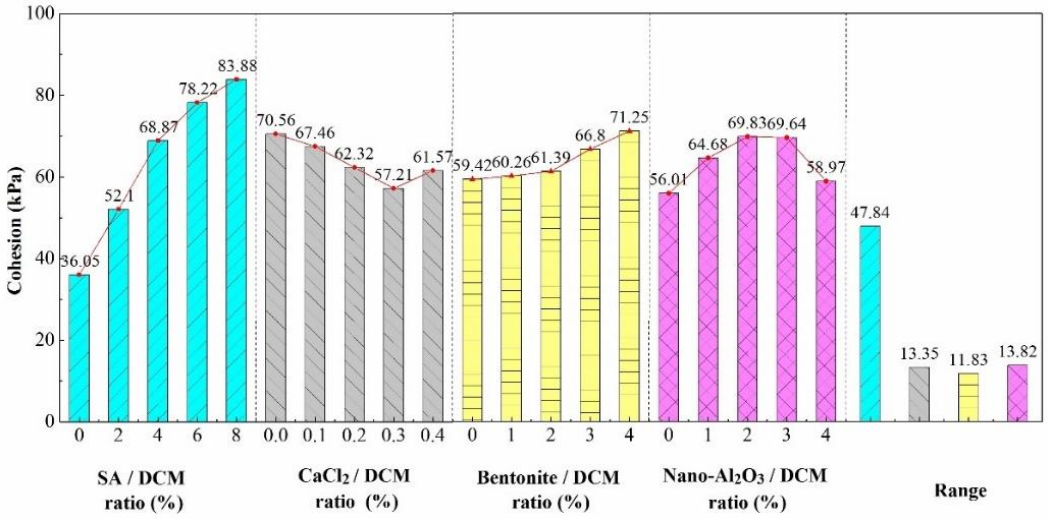

Fig. 9 Effects of mixing ratios on the cohesion of the DCM

is between 14.10° and 21.24°. The increase in the angle of internal friction is relatively small after the modification. At mixing ratios in case T14, the angle of internal friction even decreases compared with that in case 1. These results indicate that there is one or more components that are not conducive to the growth of the angle of internal friction.

Fig. 5(d) presents the coefficients of permeability of the samples measured by falling-head permeability tests. The coefficient of permeability of the plain DCM sample is 1.118×10^{-6} m/s, which is larger than those of all modified DCM samples. The average coefficient of permeability of the modified DCM (cases T2-T25) is 3.55×10^{-7} m/s, decreasing by 68.28% on average compared with that in case T1. The minimum coefficient of permeability is

2.04×10^{-7} m/s, which is obtained in case T10. A smaller coefficient of permeability can reduce the effect of rainwater on the mechanical behavior of the DCM, which is beneficial to the long-term stability of the embankment.

The above results suggest that SA, $CaCl_2$, bentonite and nano-Al_2O_3 can increase the UCS, cohesion and angle of internal friction of the DCM, and effectively reduce the coefficient of permeability of the DCM.

Fig. 6 presents the XRD patterns of plain and modified DCM. On the one hand, the amount of SA, $CaCl_2$, bentonite and nano-Al_2O_3 is very minute compared with the DCM, which makes all the high peaks identified by XRD belong to the DCM. On the other hand, the peaks of SA, $CaCl_2$, bentonite and nano-Al_2O_3 may overlap with the peaks of the DCM. Therefore, the XRD peaks of the plain and modified DCM are basically the same. To further reveal the mechanism of the modified DCM by SA, $CaCl_2$, bentonite and nano-Al_2O_3, the SEM images of the plain and modified DCM are analyzed (Figs. 7(a)-7(c)). It can be seen that the plain DCM has a loose lamellar structure with weak cementation (Fig. 7(a)). In contrast, there are spherical chain-like structures around large aggregates in the modified DCM, which increase cementation between aggregates (Fig. 7(b)). It is generally believed that $CaCl_2$ can cross-link with SA to form spherical calcium alginate (CA). Thus, the spherical chain-like structure in the modified DCM is likely the structure formed by the colloid of CA and SA. Meanwhile, the modified DCM shows many fine and regular bulk structures attached to the film formed by SA (Fig. 7(c)), which might be bentonite and nano-Al_2O_3.

Therefore, the modification of the engineering performance of the DCM may be explained in the following aspects:

• The role of SA. SA hydrogels can cement the DCM particles together to form large DCM aggregates (Rezaeimalek *et al.* 2017). Moreover, they can fill the gaps between the grains and reduce the void ratio of the DCM (Wen *et al.* 2019). Thus, SA enables to enhance the strength and reduce the coefficient of permeability.

• The role of $CaCl_2$. First, Ca^{2+} reacts with SA producing CA hydrogels, whose mechanical properties are better than those of SA hydrogels (Li *et al.* 2015). Second, the cation exchange between $CaCl_2$ and high valence cations (e.g., $Al^{3+}$and Fe^{3+}) in diffuse layers of soil particles changes the thickness of water films, reducing the soil permeability (Fu *et al.* 2019). Meanwhile, the addition of $CaCl_2$ increases the ion concentration in the free water solution between the particles, which thickens the diffuse layer of soil particles and reduces the cohesion of soil. In addition, as the dosage of $CaCl_2$ goes on increasing, $CaCl_2$ will crystallize and behave as skeletons, thus enhancing the cohesion, angle of internal friction and permeability of the DCM (Yu *et al.* 2016).

• The role of bentonite. Bentonite particles have fine sizes and large specific surface areas, so their ion-adsorption capacity is greater than that of the DCM particles (Chai *et al.* 2017). Since bentonite particles are highly hydrophilic, they are able to adsorb many water molecules and form thick water films around them (Mollins *et al.* 1996). Moreover, bentonite can serve as cementitious materials, which is able to cement the DCM particles to form many aggregates, and thus, increase the cohesion and reduce the permeability. However, after drying and water losses, the shrinkage of bentonite is greater than that of the DCM, which results in the increase of the distance between aggregates and even the formation of micro-cracks. Consequently, the UCS of the DCM is reduced. The formation of cracks increases the coefficient of permeability of the material. However, the coefficient of permeability of the modified DCM is generally smaller than that of the plain DCM because SA, $CaCl_2$, bentonite and nano-Al_2O_3 fill the microscopic pores and form hydrogels that block the water seepage channels.

• The role of nano-Al_2O_3. Nano-Al_2O_3 is a nanomaterial, which can effectively fill the tiny gaps between soil particles, and thus enhance the soil compactness (Ghasabkolaei *et al.* 2017). Because of its large specific surface area and high activity, nano-Al_2O_3 is able to form new bonds between clay particles in the DCM. This reduces the number and size of pores between clay particles, improves the microstructure of the DCM (Gao *et al.* 2015), and thus improves its UCS and cohesion. At the same time, the permeability of the DCM decreases with reducing microporosity.

Because the modification effects of SA, $CaCl_2$, bentonite and nano-Al_2O_3 are different, the modified DCM with different mixing ratios presents varied engineering performances.

4.2 Sensitivity analysis

In this section, the sensitivity analysis was conducted to evaluate the significance of each influencing factor (i.e., the SA/DCM ratio, $CaCl_2$/DCM ratio, bentonite/DCM ratio and nano-Al_2O_3/DCM ratio) on the mechanical and hydraulic properties of the modified DCM. For this purpose, the range analysis and the variance analysis were adopted.

Fig. 8 shows the results of range analysis of UCS of the modified DCM with different mixing ratios. It is observed that as the SA/DCM ratio or nano-Al_2O_3/DCM ratio increases, the UCS shows an obvious hump effect and reaches the maximum when the SA/DCM ratio is 6% or the nano-Al_2O_3/DCM ratio is 3%. As the increase in $CaCl_2$/DCM ratio, the UCS of the modified DCM also increases and reaches the maximum when the $CaCl_2$/DCM ratio is 0.3%. The UCS decreases with the increase in bentonite/DCM ratio, and the minimum is achieved when the bentonite/DCM ratio is 4%. It is also noted that the variation of the UCS affected by the SA/DCM ratio is the largest with a range of 1344.2 kPa. By contrast, the variation of the UCS affected by the nano-Al_2O_3/DCM ratio is the smallest with a range of 217.4 kPa.

Fig. 9 presents the results of range analysis of the cohesion. The cohesion is positively correlated with the SA/DCM ratio and bentonite/DCM ratio. When the SA/DCM ratio is 8% or the bentonite/DCM ratio is 4%, the cohesion of the improved DCM reaches the maximum value. As the increases in $CaCl_2$/DCM ratio, the cohesion decreases first and then increases, showing the minimum of

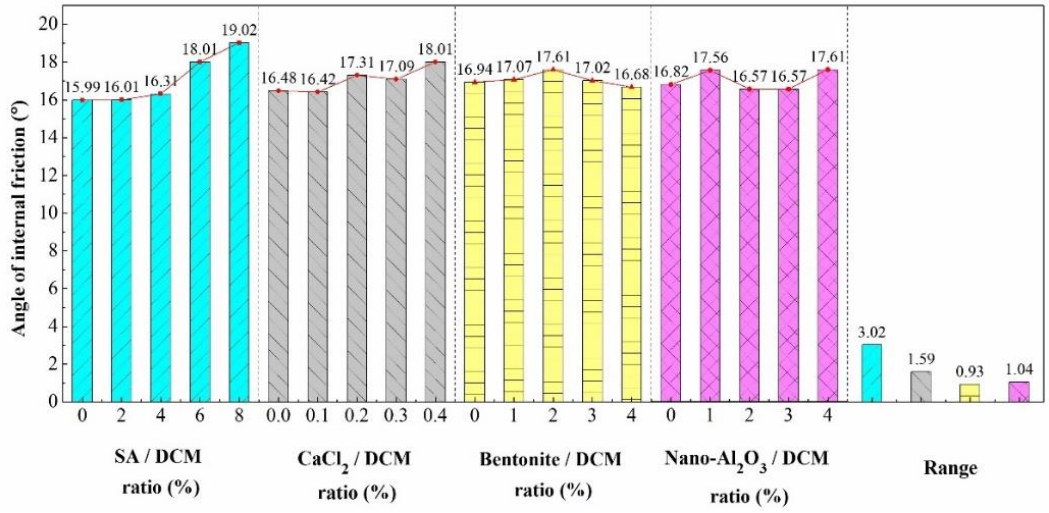

Fig. 10 Effects of mixing ratios on the angle of internal friction of the DCM

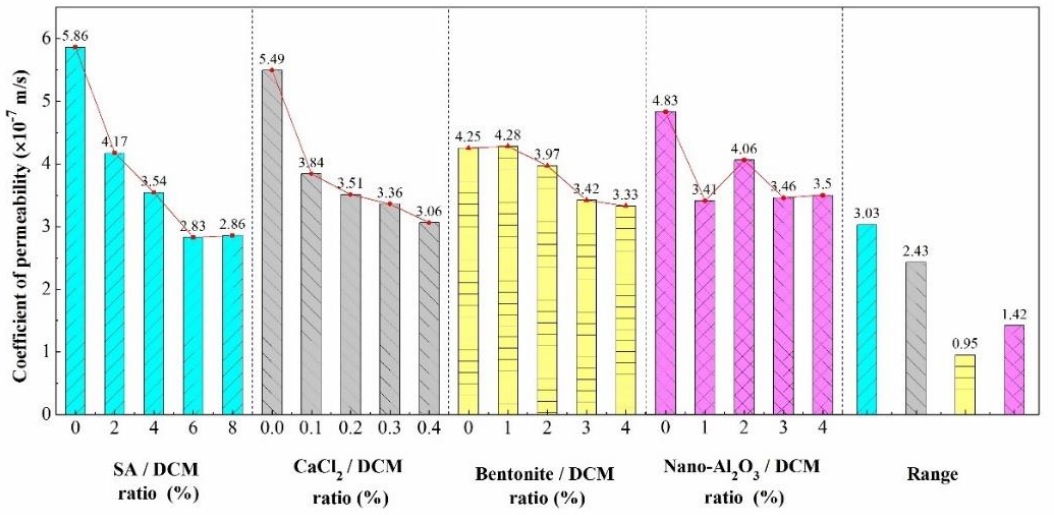

Fig. 11 Effects of mixing ratios on the coefficient of permeability of the DCM

57.21 kPa at a $CaCl_2$/DCM ratio of 0.3%. The variation of the cohesion with nano-Al_2O_3/DCM ratio shows an obvious hump effect, and the cohesion reaches the maximum when the nano-Al_2O_3/DCM ratio is 2%. The variation range of the cohesion affected by the SA/DCM ratio is the largest with a value of 47.84 kPa, and that affected by the bentonite/DCM ratio is the smallest with a value of 11.83 kPa.

The results of range analysis of the angle of internal friction are presented in Fig. 10. It is observed that the angle of internal friction shows a positive correlation with the SA/DCM ratio, reaching the maximum at an SA/DCM ratio of 8%. As the $CaCl_2$/DCM ratio increases, the angle of internal friction increases in a step-like manner and reaches the maximum when the $CaCl_2$/DCM ratio is 0.4%. The angle of internal friction increases first and then decreases with increasing bentonite/DCM ratio, and the maximum is achieved at a bentonite/DCM ratio of 2%. The angle of internal friction shows a waving trend with the increase in nano-Al_2O_3/DCM ratio, but the difference between the maximum and minimum is small (only 1.04°). One can note that SA has the greatest effect on the angle of internal friction with a variation range of 3.02°; by contrast, bentonite has the smallest effect on the angle of internal friction with a variation range of 0.93°.

Fig. 11 shows the results of range analysis of the coefficient of permeability. The coefficient of permeability of the DCM decreases first and then increases with the increase in SA/DCM ratio, and it reaches the minimum at the SA/DCM ratio of 6%. The coefficient of permeability is negatively correlated with the $CaCl_2$/DCM ratio and bentonite/DCM ratio, and it has the minimum value when the $CaCl_2$/DCM ratio is 0.4% or the bentonite/DCM ratio is 4%. On the whole, the coefficient of permeability decreases with the increase in nano-Al_2O_3/DCM ratio, and the minimum is achieved at a nano-Al_2O_3/DCM ratio of 1%. It shows that SA has the most significant effect on the coefficient of permeability with a variation range of 3.03×10^{-7} m/s, and bentonite has the smallest effect on the coefficient of permeability with a variation range of 0.95×10^{-7} m/s.

The results of variance analysis are presented in Table 3. For all the examined properties, i.e., UCS, cohesion, angle of internal friction and coefficient of permeability, SA is

Table 3 Results of variance analysis of the properties of the DCM

Property	Factor	Sum of squares	Degree of freedom	F-ratio	Significance
Unconfined compressive strength	SA/DCM ratio	5271019.50	4	27.94	*
	$CaCl_2$/DCM ratio	336393.64	4	1.78	
	Bentonite/DCM ratio	242763.44	4	1.29	
	Nano-Al_2O_3/DCM ratio	188625.49	4	1.00	
	Error	188625.49	4		
Cohesion	SA/DCM ratio	7720.13	4	15.14	*
	$CaCl_2$/DCM ratio	548.26	4	1.08	
	Bentonite/DCM ratio	509.97	4	1.00	
	Nano-Al_2O_3/DCM ratio	775.80	4	1.52	
	Error	509.97	4		
Angle of internal friction	SA/DCM ratio	37.69	4	16.19	*
	$CaCl_2$/DCM ratio	8.59	4	3.68	
	Bentonite/DCM ratio	2.33	4	1.00	
	Nano-Al_2O_3/DCM ratio	4.73	4	2.03	
	Error	2.33	4		
Coefficient of permeability	SA/DCM ratio	3.13×10^{-7}	4	7.63	*
	$CaCl_2$/DCM ratio	1.83×10^{-7}	4	4.46	
	Bentonite/DCM ratio	4.10×10^{-8}	4	1.00	
	Nano-Al_2O_3/DCM ratio	7.30×10^{-8}	4	1.78	
	Error	4.00×10^{-8}	4		

always the dominating factor with F-ratios far larger than those of other factors. Therefore, special attention should be paid to the dosage of SA when improving the DCM. By contrast, bentonite is the least important factor for most engineering properties (e.g., cohesion, angle of internal friction and coefficient of permeability) among the four factors. These findings are acceptably in agreement with those obtained from range analysis, indicating the rationality and accuracy of the results.

5. Optimal design of mixing ratios

Under the action of load and seasonal rainfall, the softening of the DCM causes the reduction of its strength, which seriously affects the safety of the DCM embankments (Zeng *et al.* 2018, Zeng *et al.* 2019, Zhang *et al.* 2019a, b). The UCS and coefficient of permeability are important indicators for the selection of embankment fillers (Liu *et al.* 2018). According to the test results, the coefficient of permeability of the modified DCM is 2.04×10^{-7}-6.22×10^{-7} m/s, indicating that the modified DCM is weakly permeable and can meet the requirement of embankment fillers. The UCS can indirectly reflect the bearing capacity of the roadbed (Patel and Patel 2012). Vanapalli *et al.* (2007) showed that the bearing capacity of unsaturated fine-grained soils can be well explained by extending the Skempton (1948) equation based on the results of unconfined compression tests. Therefore, the UCS was selected as the key evaluation indicator to determine the optimal mixing ratios in this study. According to the Chinese technical standard (CJJ/T 286-2018, 2018), the UCS of the grade I stabilized soil should reach 1500 kPa after 7 d of curing.

As shown in Fig. 6, 11 cases (i.e., T12, T13, T14, T15, T16, T18, T19, T20, T22, T23 and T25) meet the requirement that the UCS is greater than 1500 kPa. Fig. 8 presents the stress-strain curves of the modified DCM samples in these 11 cases. One can note that these samples exhibit ductile failures rather than brittle failures. The initial states and failure modes of the samples are also included in Fig. 8. The failure modes can be divided into three categories: (i) the shear failure, in cases T12, T16, T18 and T22 (see Figs. 12(a), 12(e), 12(f) and 12(i)); (ii) the shear and tensile failure, in cases T13, T14, T15, T19 and T23 (see Figs. 12(b)-12(d), 12(g) and 12(j)); and (iii) the tensile failure, in cases T20 and T25 (see Figs. 12(h) and 12(k)).

The above 11 cases (groups of mixing ratios) and test data are summarized in Table 4. It is noted that vertical, inclined and/or horizontal cracks appear on the surfaces of the samples in cases T22, T23 and T25. This is likely because SA hydrogels have a good viscosity, and they expand to some extent when encountering water. In the drying process, drying-shrinkage and polymer films are produced, which causes uneven pulling forces on the modified DCM grains. Consequently, small cracks occur on the sample surfaces and the strength of the sample is reduced. The presence of small cracks will cause the development of large cracks in the embankments, leading to great embankment deformations. Therefore, the cases T22, T23 and T25 should be avoided in engineering practice. It is also found that except for cases T22, T23 and T25, only two levels of the SA/DCM ratio (i.e., 4% and 6%) occur in the remaining eight samples, but almost every level of the other three factors are present. Therefore, the SA/DCM ratio

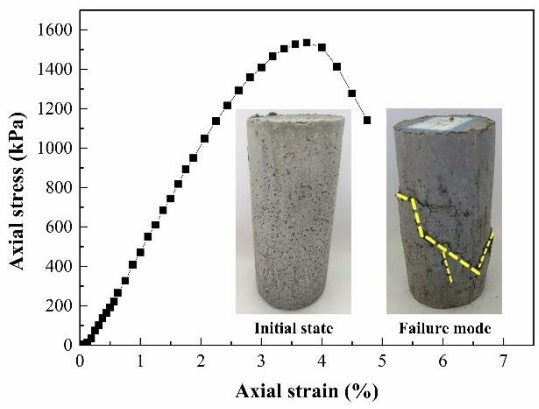

(a) T12

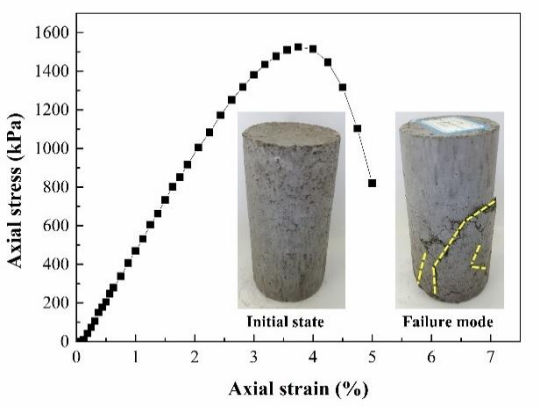

(b) T13

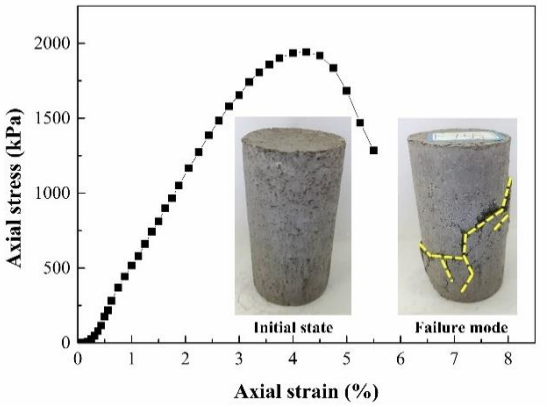

(c) T14

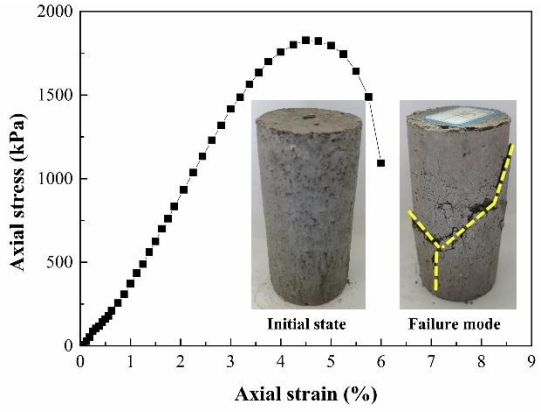

(d) T15

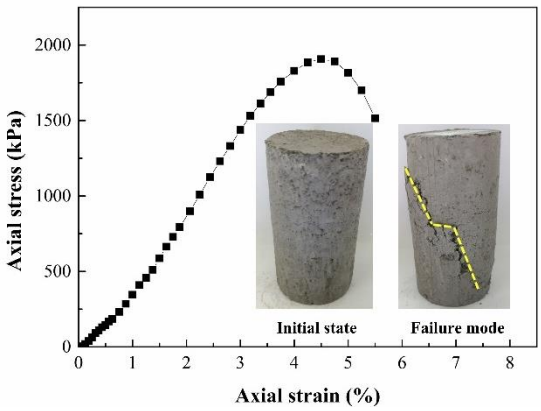

(e) T16

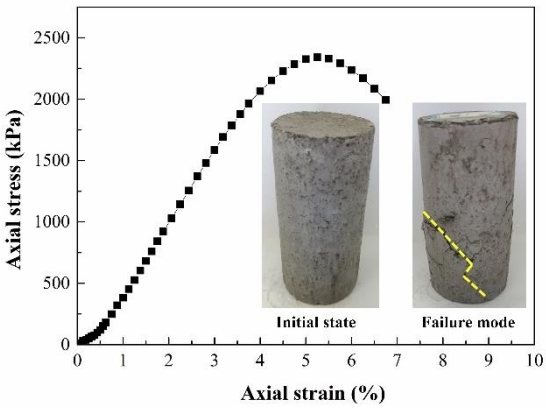

(f) T18

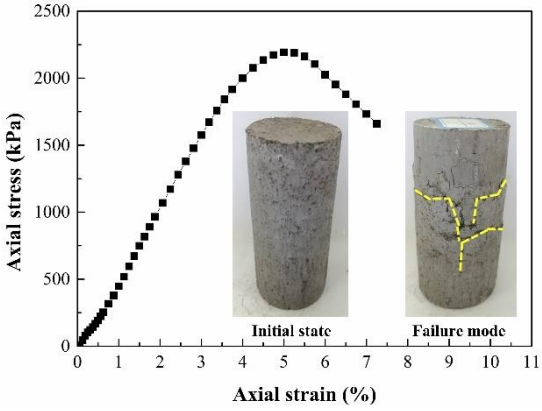

(g) T19

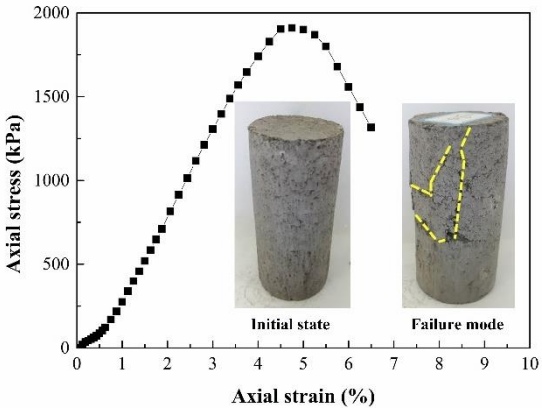

(h) T20

Fig. 12 Stress-strain curves and failure modes of the modified DCM samples in 11 cases

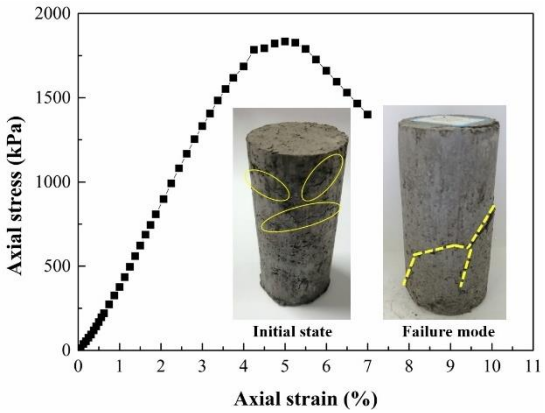

(i) T22

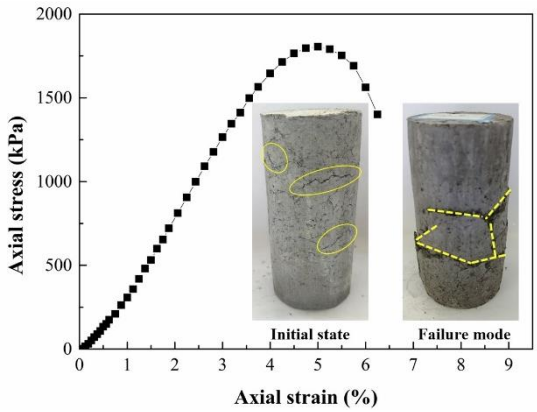

(j) T23

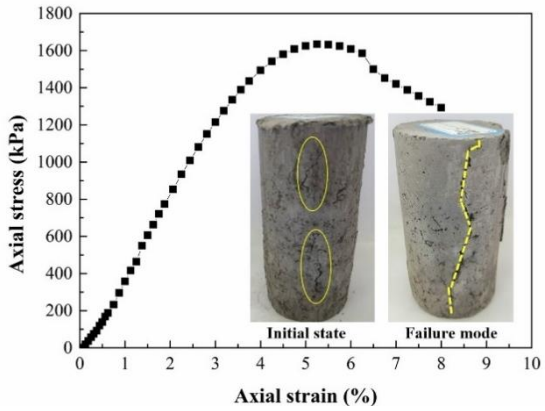

(k) T25

Fig. 12 Continued

Table 4 Summary of 11 cases and corresponding test data

Case	SA/DCM ratio (%)	$CaCl_2$/ DCM ratio(%)	Bentonite/DCM ratio(%)	Nano-Al_2O_3/DCM ratio(%)	UCS (kPa)	Cohesion (kPa)	Angle of internal friction (°)	Coefficient of permeability ($\times10^{-7}$ m/s)	Initial state	Failure mode
T12	4	0.1	3	0	1535	66.56	14.98	3.225	Intact	Shear
T13	4	0.2	4	1	1525	75.31	17.08	3.778	Intact	Shear and tensile
T14	4	0.3	0	2	1942	75.01	14.10	3.167	Intact	Shear and tensile
T15	4	0.4	1	3	1827	74.81	16.16	3.208	Intact	Shear and tensile
T16	6	0	3	1	1906	102.2	17.04	2.959	Intact	Shear
T18	6	0.2	0	3	2340	66.43	19.05	2.333	Intact	Shear
T19	6	0.3	1	4	2192	61.21	18.76	3.333	Intact	Shear and tensile
T20	6	0.4	2	0	2210	73.21	18.22	2.952	Intact	Tensile
T22	8	0.1	0	4	1833	88.03	18.54	2.550	Crack	Shear
T23	8	0.2	1	0	1805	71.21	19.43	2.952	Crack	Shear and tensile
T25	8	0.4	3	2	1634	78.02	21.24	3.430	Crack	Tensile

should be controlled in the range of 4%-6% when designing the mixing ratios, while the amount of the remaining modifier components can be adjusted reasonably according to the needs and costs.

6. Conclusions

In this study, SA, $CaCl_2$, bentonite and nano-Al_2O_3 are jointly used to modify the DCM. The orthogonal design method was employed to arrange the experiments including unconfined compression tests, direct shear tests and permeability tests. Afterward, the range analysis and variance analysis were conducted to evaluate the significance of the influences of each modifier component on the engineering properties of the modified DCM. Finally, the optimal mixing ratios for improving the performances of

the DCM were determined. The following conclusions can be drawn:

• After the treatment with the modifiers composed of SA, $CaCl_2$, bentonite and nano-Al_2O_3, the UCS, cohesive and angle of internal friction of the DCM are considerably enhanced, while the coefficient of permeability of the DCM is effectively reduced, indicating that it is feasible to use SA, $CaCl_2$, bentonite and nano-Al_2O_3 to improve the engineering performances of the DCM.

• The SA/DCM ratio is the most significant factor for all of the examined mechanical and hydraulic properties. The $CaCl_2$/DCM ratio is the second most significant factor for the UCS, angle of internal friction and coefficient of permeability, while the nano-Al_2O_3/DCM ratio is the second most significant factor for the cohesion.

• With the UCS greater than 1500 kPa as the evaluation criterion, 11 cases (groups of mixing ratios) that meet this criterion are obtained. After a further evaluation of the continuity of the sample surface in the initial state, eight satisfactory cases were finally determined for the modification of the DCM. It is recommended to use an SA/DCM ratio between 4% and 6% when designing the mixing ratio for the DCM, while the $CaCl_2$/DCM ratio, bentonite/DCM ratio and nano-Al_2O_3/DCM ratio can be properly adjusted.

Acknowledgments

This work was supported by the National Natural Science Foundation of China (Nos. 51838001, 51878070, ,51908069, 51908073 and 52008041), the Research and Development Projects in Key Fields of Hunan Province, China (No. 2019SK2171), and the Graduate Student Innovation Project of Hunan Province, China (CX 20200838).

References

ASTM. D2166/D2166M-13 (2013), Standard Test Method for Unconfined Compressive Strength of Cohesive Soil, ASTM International, West Conshohocken, Pennsylvania, U.S.A.

ASTM. D6528-07 (2007), Standard test method for consolidated undrained direct simple shear testing of cohesive soils, West Conshohocken, Pennsylvania, U.S.A.

ASTM.D5084-16a (2016), Standard Test Methods for Measurement of Hydraulic Conductivity of Saturated Porous Materials using a Flexible Wall Permeameter, ASTM International, West Conshohocken, Pennsylvania, U.S.A.

Benhouria, A., Islam, M.A., Zaghouane-Boudiaf, H., Boutahala, M. and Hameed, B.H. (2015), "Calcium alginate–bentonite–activated carbon composite beads as highly effective adsorbent for methylene blue", *Chem. Eng. J.*, **270**, 621-630. https://doi.org/10.1016/j.cej.2015.02.030.

Bhuvaneshwari, S., Robinson, R. and Gandhi, S. (2010), "Micro-fabric and mineralogical studies on the stabilization of an expansive soil using inorganic additives", *Int. J. Geotech. Eng.*, **4**(3), 395-405. https://doi.org/10.3328/IJGE.2010.04.03.395-405.

Chai, W., Huang, Y., Han, G., Liu, J., Yang, S. and Cao, Y. (2017), "An enhanced study on adsorption of Al (iii) onto bentonite and kaolin: kinetics, isotherms, and mechanisms", *Miner. Process Extr. Metall. Rev.*, **38**(2), 106-115. https://doi.org/10.1080/08827508.2016.1262862.

Chang, I., Prasidhi, A.K., Im, J. and Cho, G.C. (2015), "Soil strengthening using thermo-gelation biopolymers", *Constr. Build. Mater.*, **77**, 430-438. https://doi.org/10.1016/j.conbuildmat.2014.12.116.

CJJ/T 286-2018 (2018), Technical Standard for Application of Soil Stabilizer, Ministry of housing and construction of the People's Republic of China.

Fu, H., Liu, J., and Zha, H. (2020), "Study of the strength of disintegrated carbonaceous mudstone modified with nano-Al_2O_3 and cement", *J. Nanosci. Nanotechno.*, **20**(8), 4839-4845. https://doi.org/10.1166/jnn.2020.18486.

Fu, J.T., Hu, X.S., Li, X.L., Yu, D.M., Liu, Y.B., Yang, Y.Q. and Li, S.X. (2019), "Influences of soil moisture and salt content on loess shear strength in the Xining Basin, northeastern Qinghai-Tibet Plateau", *J. Mt. Sci.*, **16**(5), 1184-1197. https://doi.org/10.1007/s11629-018-5206-9.

Gao Q.F., Zeng L., Shi Z.N. and Zhang R. (2021), "Evolution of unsaturated shear strength and microstructure of a compacted silty clay on wetting paths", *Int. J. Geomech.*, https://doi.org/10.1061/(ASCE)GM.1943-5622.0002207.

Gao, L., Ren, Z. and Yu, X. (2015), "Experimental study of nanometer magnesium oxide-modified clay", *Soil Mech. Found. Eng.*, **52**(4), 218-224. https://doi.org/10.1007/s11204-015-9331-y.

Gao, Q.F., Dong, H., Huang, R. and Li, Z.F. (2019), "Structural characteristics and hydraulic conductivity of an eluvial-colluvial gravelly soil", *B. Eng. Geol. Environ.*, **78**(7), 5011-5028. https://doi.org/10.1007/s10064-018-01455-1.

Gao, Q.F., Shi, Z.N., Luo, J.T. and Liu, J. (2020), "Microstructural insight into permeability and water retention property of compacted binary silty clay", *J. Cent. South Univ.*, **27**(7),2068-2081. https://doi.org/10.1007/s11771-020-4431-x.

Geckil, H., Xu, F., Zhang, X., Moon, S. and Demirci, U. (2010), "Engineering hydrogels as extracellular matrix mimics", *Nanomedicine*, **5**(3), 469-484. https://doi.org/10.2217/nnm.10.12.

Ghasabkolaei, N., Choobbasti, A.J., Roshan, N. and Ghasemi, S.E. (2017), "Geotechnical properties of the soils modified with nanomaterials: A comprehensive review", *Arch. Civ. Mech. Eng.*, **17**(3), 639-650. https://doi.org/10.1016/j.acme.2017.01.010.

Gowda, R., Narendra, H., Nagabushan, B.M., Rangappa, D. and Prabhakara, R. (2017), "Investigation of nano-alumina on the effect of durability and micro-structural properties of the cement mortar", *Mater. Today P.*, **4**(11), 12191-12197. https://doi.org/10.1016/j.matpr.2017.09.149.

Guo. L.L., Zheng, D., Xu, J.C., Gao, X., Fu, X.T. and Zhang, Q. (2016), "Effects of ionic crosslinking on physical and mechanical properties of alginate mulching films", *Carbohydr. Polym.*, **136**, 259-265. https://doi.org/10.1016/j.carbpol.2015.09.034.

Hataf N, Ghadir P. and Ranjbar N. (2018), "Investigation of soil stabilization using chitosan biopolymer", *J. Clean. Prod.*, **170**, 1493-1500. https://doi.org/10.1016/j.jclepro.2017.09.256.

Hecht, H. and Srebnik, S. (2016), "Structural characterization of sodium alginate and calcium alginate", *Biomacromolecules*, **17**(6), 2160-2167. https://doi.org/10.1021/acs.biomac.6b00378.

Hu, J., Zhang, L., Wei, H. and Du, J. (2018), "Experimental study of the compressive strength of chemically reinforced organic-sandy soil", *Geomech. Eng.*, **16**(3), 247-255. https://doi.org/10.12989/gae.2018.16.3.247.

Indraratna, B., Athukorala, R. and Vinod, J. (2012), "Estimating the rate of erosion of a silty sand treated with lignosulfonate", *J.*

Geotech. Geoenviron. Eng., **139**(5), 701-714. https://doi.org/10.1061/(ASCE)GT.1943-5606.0000766.

Jin, D., Guan, Z., Huo, L. and Wang, X. (2017), "Possible impacts of spring sea surface temperature anomalies over South Indian Ocean on summer rainfall in Guangdong-Guangxi region of China", *Clim. Dynam.*, **49**(9), 3075-3090. https://doi.org/10.1007/s00382-016-3494-8.

Kumar S.A. and Sujatha E.R. (2021), "An appraisal of the hydro-mechanical behaviour of polysaccharides, xanthan gum, guar gum and β-glucan amended soil", *Carbohyd. Polym.*, **265**, 118083. https://doi.org/10.1016/j.carbpol.2021.118083.

Lee, S., Chang, I., Chung, M.K., Kim, Y. and Kee, J. (2017), "Geotechnical shear behavior of xanthan gum biopolymer treated sand from direct shear testing", *Geomech. Eng.*, **12**(5), 831-847. https://doi.org/10.12989/gae.2017.12.5.831.

Li, J., He, J., Huang, Y., Li, D. and Chen, X. (2015), "Improving surface and mechanical properties of alginate films by using ethanol as a co-solvent during external gelation", *Carbohyd. Polym.*, **123**, 208-216. https://doi.org/10.1016/j.carbpol.2015.01.040.

Liu, L., Qiao, J., Shen, B., Lu, X. and Yang, Y. (2017), "Geological characteristics and shale gas distribution of carboniferous mudstones in the Tarim Basin, China", *Acta Geochim.*, **36**(2) 260-275. https://doi.org/10.1007/s11631-017-0144-8.

Liu, S., Li, Z., Li, Y. and Cao, W. (2018), "Strength properties of Bayer red mud stabilized by lime-fly ash using orthogonal experiments", *Constr. Build. Mater.*, **166**, 554-563. https://doi.org/10.1016/j.conbuildmat.2018.01.186.

Liu, Z. (2015), "Influence of rainfall characteristics on the infiltration moisture field of highway subgrades", *Road Mater. Pavement Des.*, **16**(3) 635-652. https://doi.org/10.1080/14680629.2015.1021370.

Luo, H.L., Hsiao, D.H., Lin, D.F. and Lin, C.K. (2012), "Cohesive soil stabilized using sewage sludge ash/cement and nano-Al_2O_3", *Int. J. Transp. Sci. Technol.*, **1**(1), 83-99. https://doi.org/10.1260/2046-0430.1.1.83.

Luo, H.L., Lin, D.F., Shieh, S.I. and You, Y.F. (2015), "Micro-observations of different types of nano-Al_2O_3 on the hydration of cement paste with sludge ash replacement", *Environ. Technol.*, **36**(23), 2967-2976. https://doi.org/10.1080/09593330.2014.911362.

Mollins, L.H., Stewart, D.I. and Cousens, T.W. (1996), "Predicting the properties of bentonite-sand mixtures", *Clay. Miner.*, **31**(2), 243-252. https://doi.org/10.1180/claymin.1996.031.2.10.

Mujah, D., Shahin, M.A. and Cheng, L. (2017), "State-of-the-art review of biocementation by microbially induced calcite precipitation (MICP) for soil stabilization", *Geomicrobiol. J.*, **34**(6). 524-537. https://doi.org/10.1080/01490451.2016.1225866.

Patel M.A. and Patel H. (2012), "Experimental study to correlate the test results of PBT, UCS, and CBR with DCP on various soils in soaked condition", *Int. J. Eng.*, **6**(5):244.

Rezaeimalek, S., Huang, J. and Bin-Shafique, S. (2017), "Performance evaluation for polymer-stabilized soils", *Transp. Res. Record.*, **2657**(1), 58-66. https://doi.org/10.3141/2657-07.

Sarika, P.R. and James, N.R. (2016), "Polyelectrolyte complex nanoparticles from cationised gelatin and sodium alginate for curcumin delivery", *Carbohydr. Polym.*, **148**, 354-361. https://doi.org/10.1016/j.carbpol.2016.04.073.

Tan, T.S., Goh, T.L. and Yong, K.Y. (2002), "Properties of Singapore marine clays improved by cement mixing", *Geotech. Test. J.*, **25**(4), 422-433. https://doi.org/10.1520/GTJ11295J.

Taylor-Lange, S.C., Lamon, E.L., Riding, K.A. and Juenger, M.C. (2015), "Calcined kaolinite–bentonite clay blends as supplementary cementitious materials", *Appl. Clay Sci.*, **108**, 84-93. https://doi.org/10.1016/j.clay.2015.01.025.

Vanapalli, S.K., Oh, W.T. and Puppala, A.J. (2007), "Determination of the bearing capacity of unsaturated soils under undrained loading conditions", *Proceedings of the 60th Canadian Geotechnical Conference*, Ottawa, Canada, October.

Voottipruex, P. and Jamsawang, P. (2014), "Characteristics of expansive soils improved with cement and fly ash in Northern Thailand", *Geomech. Eng.*, **6**(5), 437-453. https://doi.org/10.12989/gae.2014.6.5.437.

Wen, K., Li, Y., Huang, W., Armwood, C., Amini, F. and Li, L. (2019), "Mechanical behaviors of hydrogel-impregnated sand", *Constr. Build. Mater.*, **207**, 174-180. https://doi.org/10.1016/j.conbuildmat.2019.02.141.

Xiao, Y., Stuedlein, A.W., Chen, Q., Liu, H. and Liu, P. (2017), "Stress-strain-strength response and ductility of gravels improved by polyurethane foam adhesive", *J. Geotech. Geoenviron. Eng.*, **144**(2), 04017108. https://doi.org/10.1061/(ASCE)GT.1943-5606.0001812.

Xiao, Z., Wang, Z., Huang, M., Luo, X., Liang, Y. and Lin, Z. (2020), "Urbanization in an underdeveloped city—Nanning, China and its impact on a heavy rainfall event in July". *Earth Sp. Sci.*, **7**(4), e2019EA000991. https://doi.org/10.1029/2019EA000991.

Yu, Z. H., Liu, X. M., Xu, C.Y., Xiong, H.L. and Li, H. (2016), "Specific ion effects on soil water movement", *Soil Till. Res.*, **161**, 63-70. https://doi.org/10.1016/j.still.2016.03.004.

Zeng, L., Bian, H.B., Shi, Z.N. and He Z.M. (2017), "Forming condition of transient saturated zone and its distribution in residual slope under rainfall conditions", *J. Cent. South Univ.*, **24**(8), 1866-1880. https://doi.org/10.1007/s11771-017-3594-6.

Zeng, L., Luo, J.T., Liu, J., Gao, Q.F. and Bian, H.B. (2021a), "Disintegration characteristics and mechanisms of carbonaceous mudstone subjected to load and cyclic drying-wetting", *J. Mater. Civ. Eng.*, **33**(8), 04021195. https://doi.org/10.1061/(ASCE) MT.1943-5533.0003817.

Zeng, L., Xiao, L.Y., Zhang, J.H. and Gao, Q.F. (2019), "Effect of the characteristics of surface cracks on the transient saturated zones in colluvial soil slopes during rainfall", *B. Eng. Geol. Environ.*, 1-11. https://doi.org/10.1007/s10064-019-01584-1.

Zeng, L., Yu, H. C., Liu, J., Gao, Q. F., and Bian, H. B. (2021b), "Mechanical behaviour of disintegrated carbonaceous mudstone under stress and cyclic drying/wetting", *Constr. Build. Mater.*, **282**, 122656. https://doi.org/10.1016/j.conbuildmat.2021.122656.

Zhang, J.H., Gu, F. and Zhang, Y. (2019b), "Use of building-related construction and demolition wastes in highway embankment: Laboratory and field evluations", *J. Clean. Prod.*, **230**, 1051-1060. https://doi.org/10.1016/j.jclepro.2019.05.182.

Zhang, J.H., Peng, J.H. Zeng, L., Li J. and Li, F. (2019a), "Rapid estimation of resilient modulus of subgrade soils using performance-related soil properties", *Int. J. Pavement. Eng.*, 1-8. https://doi.org/10.1080/10298436.2019.1643022.

Zhang, M., Guo, H., El-Korchi, T., Zhang, G. and Tao, M. (2013), "Experimental feasibility study of geopolymer as the next-generation soil stabilizer", *Constr. Build. Mater.*, **47**, 1468-1478. https://doi.org/10.1016/j.conbuildmat.2013.06.017.

Zhang, T., Cai, G. and Liu, S. (2018), "Application of lignin-stabilized silty soil in highway subgrade: A macroscale laboratory study", *J. Mater. Civ. Eng.*, **30**(4), 04018034. https://doi.org/10.1061/(ASCE)MT.1943-5533.0002203.

CC